Magnetic Resonance Imaging 33 (2015) 1106–1113

Contents lists available at ScienceDirect

Magnetic Resonance Imaging

journal homepage: www.mrijournal.com

Image reconstruction from phased-array data based on multichannel blind deconvolution

Huajun She [a], Rong-Rong Chen [a], Dong Liang [b], Yuchou Chang [c], Leslie Ying [d,*]

[a] Department of Electrical and Computer Engineering, University of Utah, Salt Lake City, UT 84112
[b] Paul C. Lauterbur Research Center for Biomedical Imaging, Shenzhen Key Laboratory for MRI, Institute of Biomedical and Health Engineering, Shenzhen Institutes of Advanced Technology, Chinese Academy of Sciences, Shenzhen, P.R. China
[c] Neuroimaging Research, Barrow Neurological Institute, Phoenix, AZ 85013
[d] Department of Biomedical Engineering, Department of Electrical Engineering, The State University of New York at Buffalo, Buffalo, NY 14260

ARTICLE INFO

Article history:
Received 14 January 2015
Revised 4 June 2015
Accepted 20 June 2015

Keywords:
Phased array coils
Non-uniform intensity
Multichannel blind deconvolution
Regularization
Image restoration

ABSTRACT

In this paper we consider image reconstruction from fully sampled multichannel phased array MRI data without knowledge of the coil sensitivities. To overcome the non-uniformity of the conventional sum-of-square reconstruction, a new framework based on multichannel blind deconvolution (MBD) is developed for joint estimation of the image function and the sensitivity functions in image domain. The proposed approach addresses the non-uniqueness of the MBD problem by exploiting the smoothness of both functions in the image domain through regularization. Results using simulation, phantom and *in vivo* experiments demonstrate that the reconstructions by the proposed algorithm are more uniform than those by the existing methods.

1. Introduction

MRI using phased array coils has emerged as a powerful technique to improve signal-to-noise ratio (SNR) of an image [1], reduce image acquisition time [2–4], or remove artifacts [5]. With phased array coils, the acquired images usually have non-uniform intensity due to the coil sensitivity weighting. Removal of the sensitivity weighting for the original image requires prior knowledge of the sensitivities of the receiver coils [1,6,7]. A typical method to reconstruct the original image without such prior information is the sum-of-squares (SOS) method [1]. Other combination approaches [8–10] have also been proposed to improve SNR. For the SOS method, the reconstructed image is obtained by taking the square root of the sum of the absolute squares of the multiple images acquired with phased array coils. The SOS method effectively removes the spatially varying sensitivity weighting under the key assumption that the sum of the absolute squares of all sensitivity functions is spatially uniform. This assumption, however, is usually violated with surface coils, and the reconstructed image tends to be dark at locations further away from all coils (e.g., the center of the array). The non-uniformity of the image intensity greatly complicates further automatic analysis such as registration and tissue segmentation [11]. Although non-uniform intensity of single-coil images has been addressed by numerous works (e.g., [11] and references therein), few [12,13] have studied the issue in the context of multi-coil images. In [12], an l_p norm was used in replace of the l_2 norm in the SOS reconstruction to improve the uniformity, based on the assumption that the l_p norm of the sensitivity is uniform. The accuracy of such assumption, however, depends on specific coil structures. Another method in [13] is based on a multichannel blind deconvolution (MBD) framework [14–16], treating both the original image and the sensitivity functions as unknowns to be reconstructed simultaneously. It adopts a subspace-based MBD method to perform deconvolution in the image domain and assumes a polynomial model for the sensitivity functions. A limitation of the method is that it is sensitive to noise, and typically high-SNR acquisitions are needed for uniform reconstructions. Compared to [12], the MBD approach in [13] does not impose any uniformity constraint on the combined coil sensitivities.

In this paper, we propose a new approach to reconstruct the original uniform image using fully sampled multichannel data. Inspired by an approach developed previously for image super-resolution [17], the proposed method uses regularizations to address the non-uniqueness of the solutions, which utilize the prior information that the image and sensitivity functions are smooth in the image domain.

* Corresponding author at: Department of Biomedical Engineering, Department of Electrical Engineering, The State University of New York at Buffalo, 223 Davis Hall, Buffalo, NY 14260. Tel.: +1 716 645 1609.
E-mail address: leiying@buffalo.edu (L. Ying).

http://dx.doi.org/10.1016/j.mri.2015.06.008
0730-725X/

2. Theory

2.1. Summary of the MBD structure

In MRI with phased array coils, the *k*-space data are acquired simultaneously from *L* receiver coils with different sensitivities. The acquired data are the Fourier transform of the sensitivity-weighted images. The imaging equation is given by

$$Y_i\left(k_x,k_y\right)=\iint f(x,y)h_i(x,y)e^{-j2\pi\left(k_x x+k_y y\right)}dxdy, \tag{1}$$

where (x,y) are image domain coordinates, $f(x,y)$ is the desired object image, $h_i(x,y)$ are the sensitivity functions for the i-th coil ($i=1,2,\cdots,L$), (k_x,k_y) are k-space domain coordinates, $Y_i(k_x,k_y)$ are the k-space sampling data collected from the i-th coil. The discretized sensitivity-weighted image represented by

$$y_i(m,n)=f(m,n)h_i(m,n) \tag{2}$$

can be obtained by taking the inverse discrete Fourier transform (IDFT) of the acquired *k*-space data sampled above the Nyquist rate. When both the original image $f(m,n)$ and the sensitivity functions $h_i(m,n)$ are unknown, the problem of reconstructing the original image from the output $y_i(m,n)$ can be handled in the MBD framework.

2.2. Subspace approach and maximum-likelihood approach

Two approaches are widely used for MBD image reconstruction. The first approach is the maximum-likelihood method [14], named ML-MBD here, which utilizes the data consistency in measurements in Eq. (2). The second one for MBD is the subspace method [15,16], named Subspace-MBD here, which utilizes the property, referred to as the cross-relation, that in the absence of noise, if the output of the i-th channel is put into the j-th channel, then the signal generated is the same as that generated by putting the output of the j-th channel into the i-th channel. According to the properties of DFT, these *k*-space data are the circular convolution of the original image and the sensitivity functions, both in *k*-space:

$$Y_i(k_m,k_n)=F(k_m,k_n)*H_i(k_m,k_n), \tag{3}$$

where "*" denotes 2-D circular convolution. Therefore mathematically, we have

$$Y_i*H_j-Y_j*H_i=0, \tag{4}$$

where H_i and H_j are Fourier transform of h_i and h_j, and "*" is the convolution operator. Combining Eq. (3) for all (i,j) pairs, we obtain a set of equations which can be used to solve for the sensitivity functions H_i given the acquired data. The Subspace-MBD approach was adopted in [13] where the sensitivity functions are modeled as polynomials in the image domain. Since multiplication of polynomials becomes a linear convolution between the polynomial coefficients, the Subspace-MBD method was employed. However, the Subspace-MBD approach is known to be sensitive to noise, which is also demonstrated in the Results section.

For our case of interest, we observe that the solutions to both Eqs. (3) and (4) are not unique. To see this, we first show that the SOS reconstruction is always a solution to Eqs. (3) and (4). Let us consider the SOS reconstruction

$$f_{\text{sos}}(m,n)=\sqrt{\sum_{i=1}^{L}|y_i(m,n)|^2}, \tag{5}$$

and the corresponding sensitivity function given by

$$h_{\text{sos},i}(m,n)=\frac{y_i(m,n)}{f_{\text{sos}}(m,n)},\quad i=1,\cdots,L. \tag{6}$$

It follows that

$$y_i(m,n)=f_{\text{sos}}(m,n)h_{\text{sos},i}(m,n), \tag{7}$$

and equivalently in *k*-space

$$Y_i(k_m,k_n)=F_{\text{sos}}(k_m,k_n)*H_{\text{sos},i}(k_m,k_n). \tag{8}$$

This verifies that the SOS reconstruction is a solution to Eq. (3). One can further verify that the following cross- relation holds:

$$Y_j(k_m,k_n)*H_{\text{sos},i}(k_m,k_n)=Y_i(k_m,k_n)*H_{\text{sos},j}(k_m,k_n), \tag{9}$$

which suggests that the SOS reconstruction is also a solution to the cross-relation Eq. (4). It is easily seen that when we multiply a particular pixel of the SOS image $f_{\text{sos}}(m,n)$ by γ, and multiply the corresponding pixel of sensitivity function $h_{\text{sos},i}(m,n)$ by $1/\gamma$ to obtain a new pair of $f(m,n)$ and $h_i(m,n)$, the new pair is still a solution to Eqs. (3) and (4). This confirms the non-uniqueness of both the ML-MBD and Subspace-MBD methods for our case of interest.

2.3. P-norm approach

The p-norm approach is a generalization of the traditional SOS method. SOS is simple to implement and has nearly optimal SNR, but may still lead to inhomogeneous images. The p-norm combination is given by

$$f_{\text{pnorm}}(m,n)=\left(\sum_{i=1}^{L}|y_i(m,n)|^p\right)^{1/p}. \tag{10}$$

After the p-norm combination is computed, a constrained optimization problem is solved to estimate the vectorized optimal sensitivity function $\vec{h}$:

$$\arg\min_{\vec{h}_i}\sum_{i=1}^{L}\left\|\text{diag}\left(\vec{f}_{\text{pnorm}}\right)\vec{h}_i-\vec{y}_i\right\|^2+\lambda\sum_{i=1}^{L}R\left(\vec{h}_i\right), \tag{11}$$

where $\vec{y}_i$ is the vectorized image data, $\vec{f}_{\text{pnorm}}$ is the vectorized p-norm combination, diag(•) denotes putting the vector into the diagonal of the matrix, and $\vec{h}_i$ is the vectorized sensitivity function, and $R(\vec{h}_i)$ is the total variation regularization term of the sensitivity functions. Then the estimated sensitivities are used to compute the weights:

$$w_i(m,n)=\frac{h_i^*(m,n)}{\sum_i|h_i(m,n)|^2}, \tag{12}$$

where $(\cdot)^*$ is the conjugate operator. These weights are finally used to compute the optimal linearly combined image [1]

$$f_{\text{opt}}(m,n)=\sum_i w_i(m,n)y_i(m,n). \tag{13}$$

The p-norm combination may improve image homogeneity in noise free environment [12]. However, with image noise, SNR of f_{opt} is degraded after the p-norm combination [12].

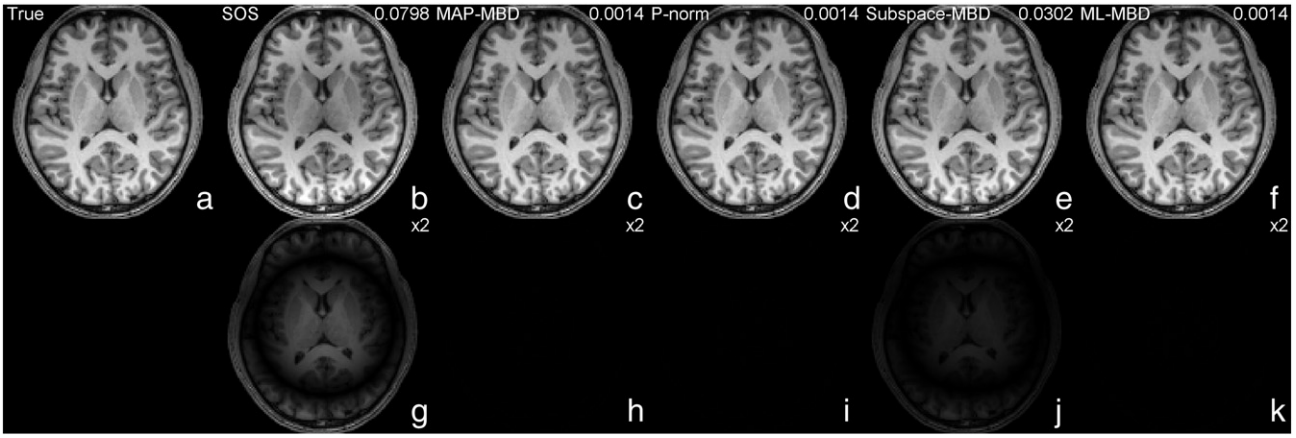

Fig. 1. Simulation results for a 128 × 128 image reconstructed from a set of 8-channel data. The first row shows the true image and the reconstructed images using the proposed MAP-MBD, p-norm, Subspace-MBD and ML-MBD methods. The nRMSE is shown on each subfigure. The second row shows the difference images between each reconstruction and the true image. It is observed that the SOS reconstruction is the darkest in the central region and thus it exhibits the largest difference from the true image. The difference image of the Subspace-MBD method is also quite noticeable. Since this simulated dataset is noise free, the proposed MAP-MBD method, the p-norm method and the ML-MBD method perform similarly in both the visual image quality and the nRMSE.

2.4. MAP-MBD approach

Given the non-uniqueness of the ML-MBD approach, we propose a new approach which employs regularization in the maximum likelihood method to resolve the ambiguity in non-unique solutions. Two regularization terms are used with one for the image function and the other for the sensitivity functions, both incorporating smoothness constraint in the image domain. The proposed method can be equivalently regarded as a maximum a posteriori (MAP) method with known prior [18], and is thereby named the MAP-MBD approach. To estimate the vectorized image $\vec{f}$ and sensitivity functions $\vec{h}_i, i = 1,\ldots,L$, we minimize an objective function defined as

$$E\left(\vec{f},\vec{h}_i\right)=\sum_{i=1}^{L}\left\|\mathrm{diag}\left(\vec{h}_i\right)\vec{f}-\vec{y}_i\right\|^2+\alpha R\left(\vec{f}\right)+\beta\sum_{i=1}^{L}R\left(\vec{h}_i\right). \quad (14)$$

The first data consistency term measures the fidelity to the data and comes from the acquisition model in Eq. (2). The last two regularization terms utilize the smoothness of the image and the sensitivity functions in the image domain. $R(\vec{f})$ is the l_2 norm of the finite difference of the image defined as

$$R\left(\vec{f}\right)=\vec{f}^{H}\Lambda\vec{f}, \quad (15)$$

where Λ is a positive semi-definite block tri-diagonal Laplacian matrix. The parameters α and β are adjusted to control the convergence and smoothness of the solution to Eq. (14).

2.5. Alternative minimization

It follows from Eq. (14) that the objective function can be written as

$$E\left(\vec{f},\vec{h}_i\right)=\sum_{i=1}^{L}\left\|\mathrm{diag}\left(\vec{h}_i\right)\vec{f}-\vec{y}_i\right\|^2+\alpha\vec{f}^{T}\Lambda\vec{f}+\beta\sum_{i=1}^{L}\vec{h}_i^{T}\Lambda\vec{h}_i. \quad (16)$$

As a function of both $\vec{f}$ and $\vec{h}_i$, the objective function E in Eq. (16) is not a convex function. However, E is convex with respect to $\vec{f}$ if $\vec{h}_i$ is fixed and is also convex with respect to $\vec{h}_i$ if $\vec{f}$ is fixed. Thus, the optimization problem can be solved by an alternative minimization (AM) method [17,19], which computes a minimization sequence $(\vec{f}^{m},\vec{h}_i^{m})$ alternatively. In the following two-step approach we compute the derivatives with respect to $\vec{f}$ and $\vec{h}_i$, respectively, and set them to be zero to find the minimizing values. After initialized with $\vec{f}^{0}$ and $\vec{h}^{0}$, the m-th iteration is performed as follows

f-step:

$$\begin{aligned}\vec{f}^{m}&=\arg\min_{\vec{f}}E\left(\vec{f},\vec{h}^{m-1}\right)\Rightarrow\frac{\partial E}{\partial\vec{f}} \quad (17)\\&=0\Leftrightarrow\sum_{i=1}^{L}2\left[\mathrm{diag}\left(\vec{h}_i^{m-1}\right)\right]^{*}\left(\mathrm{diag}\left(\vec{h}_i^{m-1}\right)\vec{f}-\vec{y}_i\right)+\alpha\Lambda\vec{f}=0,\end{aligned}$$

h-step:

$$\begin{aligned}\vec{h}_i^{m}&=\arg\min_{\vec{h}_i}E\left(\vec{f}^{m},\vec{h}_i\right)\Rightarrow\frac{\partial E}{\partial\vec{h}_i} \quad (18)\\&=0\Leftrightarrow2\left[\mathrm{diag}\left(\vec{f}^{m}\right)\right]^{*}\left(\mathrm{diag}\left(\vec{f}^{m}\right)\vec{h}_i-\vec{y}_i\right)+\beta\Lambda\vec{h}_i=0,\end{aligned}$$

where $(\cdot)^*$ is the conjugate operator.

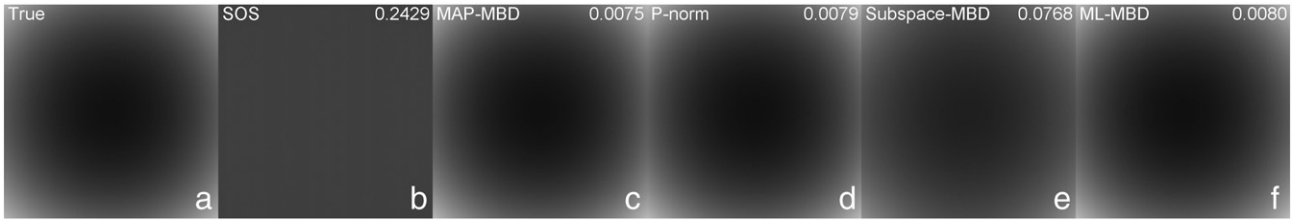

Fig. 2. Images for the sum-of-squares of the true and estimated sensitivity functions obtained from various methods. The combined sensitivity functions from the proposed, p-norm and ML-MBD methods show similar spatial variation to the true one, while those from the SOS and Subspace-MBD methods are not as close, as seen visually and also suggested by the nRMSE.

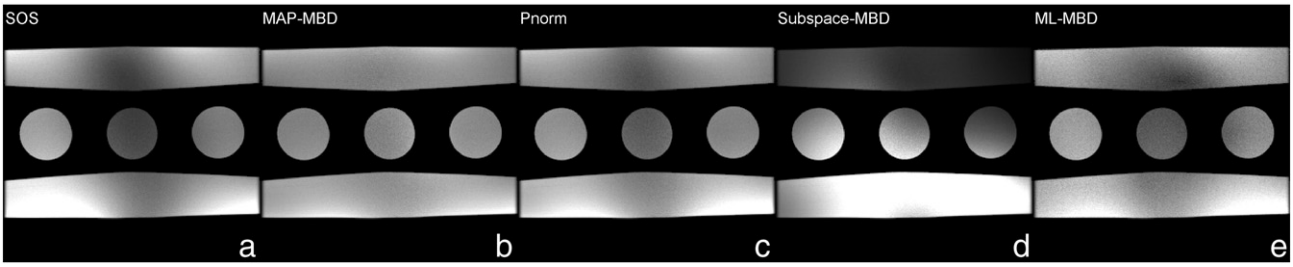

Fig. 3. Experimental results from a set of phantom data. The image intensity of the proposed MAP-MBD method is more uniform than that of the SOS, p-norm, Subspace-MBD and ML-MBD methods.

3. Methods

The proposed MAP-MBD method was evaluated on four T1-weighted datasets: simulated data, phantom data, *in vivo* brain data, and *in vivo* cardiac data. All reconstruction methods were implemented in MATLAB (MathWorks, Natick, MA) on a workstation (Hewlett-Packard, Palo Alto, CA). The SOS reconstruction, the p-norm reconstruction, the Subspace-MBD reconstruction and the ML-MBD reconstruction are provided for comparison. All reconstructed images for the same dataset are normalized and shown individually on the same scale for visual evaluations of uniformity in intensity.

3.1. Simulation

A 128×128 MR image is used as the original image. The simulated *k*-space data (noise free) were generated by Fourier transforming the images weighted by a set of eight sensitivity functions. The sensitivity functions were simulated using the Biot–Savart law [20]. The objective of this simulation experiment is to study the effectiveness of the proposed method under noise-free measurements. The proposed method is compared with the SOS, Subspace-MBD, p-norm and ML-MBD methods with the true image as the reference. The values for the regularization parameters are: $\alpha = 1 \times 10^{-5}$, $\beta = 1 \times 10^{-2}$ for the proposed method.

3.2. Phantom experiment

The objective of the phantom experiment is to demonstrate that the proposed method can generate uniform intensity in reconstructions. A phantom that is piecewise-constant was used for easy identification of non-uniformity. A T1-weighted scan was performed on the phantom using a two-dimensional spin echo sequence on a 3 T commercial scanner (GE Healthcare, Waukesha, WI) with an four-channel torso coil (echo time/pulse repetition time = 11/300 ms, FOV = 18 × 18 cm, matrix = 256 × 256, slice thickness = 1.7 mm). For comparison, SOS, MAP-MBD, Subspace-MBD with polynomial model, p-norm and ML-MBD methods were used for reconstruction. The regularization parameters are: $\alpha = 1 \times 10^{-5}$, $\beta = 1 \times 10^{2}$ for the proposed method.

3.3. In vivo human brain imaging experiment

This experiment is to examine the performance of the proposed method when applied to *in vivo* data. One set of sagittal *in vivo* human brain data was acquired. The sagittal data set was on a GE 3 T scanner (GE Healthcare, Waukesha, WI) with a four-channel head coil and a 3D T1-weighted spoiled gradient echo sequence (TE = minimum full, TR = 7.5 ms, FOV = 24 × 24 cm, matrix = 256 × 256, slice thickness = 1.7 mm). Informed consent was obtained from the volunteer in accordance with the institutional review board policy. Similar to the phantom study, the SOS, MAP-MBD, Subspace-MBD, p-norm and ML-MBD methods were used for performance comparison. The values for the regularization parameters are: $\alpha = 1 \times 10^{-5}$, $\beta = 1 \times 10^{4}$ for the proposed method.

3.4. In vivo cardiac imaging experiment

This experiment is to examine the performance of the proposed method when applied to one frame of *in vivo* cardiac data, where air-tissue boundaries might induce sharp transitions in the estimated coil sensitivities for traditional methods. The dataset was acquired from a 3 T scanner (Siemens Trio, Erlangen, Germany), with a 12 channel phased array coil (combined to 4 coils), using a 2D true FISP sequence (TE = 1.87 ms, TR = 29.9 ms, BW = 930, flip = 50°, FOV = 34 × 28.6875 cm, matrix = 256 × 216, slice thickness = 6 mm). The SOS, MAP-MBD, Subspace-MBD, p-norm and ML-MBD methods were used for performance comparison. The values for the regularization parameters are: $\alpha = 1 \times 10^{-4}$, $\beta = 1 \times 10^{4}$ for the proposed method.

3.5. Parameters selection

For the proposed method, different regularization parameters are needed for optimization. Regarding the choice of parameters, we find: (a) the parameters should be chosen such that the three terms

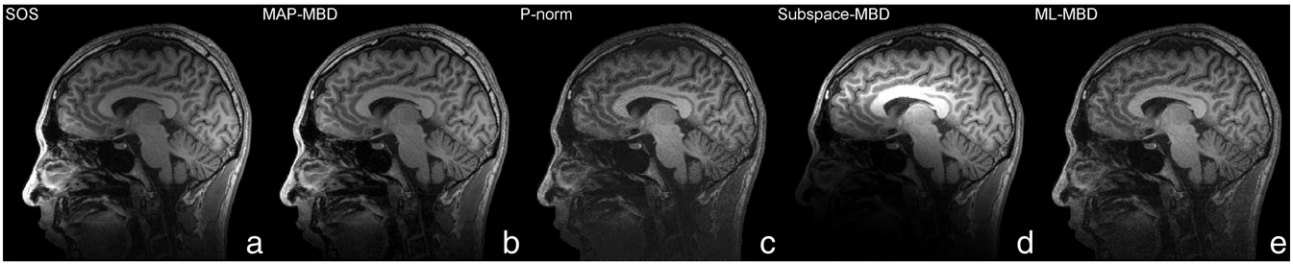

Fig. 4. Experimental results from a set of *in vivo* sagittal brain data. The higher level of uniformity in the proposed method makes image details more visible in the central upper part of the brain image when compared with the SOS method. The Subspace-MBD reconstruction is very dark towards the neck. The p-norm and ML-MBD reconstructions are much noisier than the MAP-MBD reconstruction.

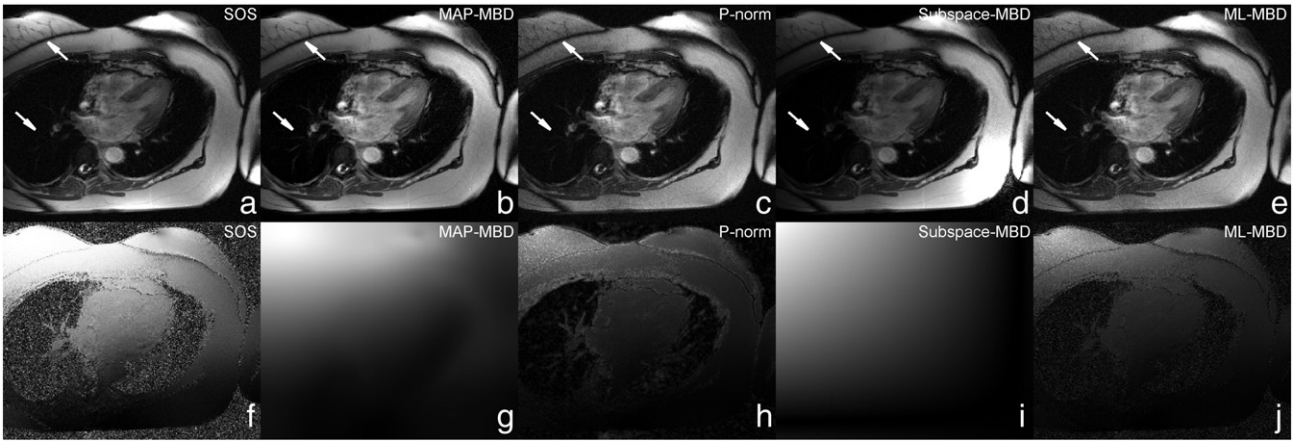

Fig. 5. Experimental results from a set of *in vivo* cardiac data. The top row compares the reconstructions and the bottom row compares the sensitivities of a coil near the air-tissue interface for all methods. The central regions of the SOS reconstruction and the Subspace-MBD reconstruction are both darker than that of the proposed MAP-MBD method. The higher level of uniformity in the MAP-MBD method makes image details around the heart more visible (indicated by the lower white arrow) than that of the SOS and the Subspace-MBD methods. The p-norm and ML-MBD reconstructions are noisier than that of the MAP-MBD method, especially at the front and back of the chest (indicated by the upper white arrow). The MAP-MBD provides a smooth and clean estimation of the sensitivity, which agrees with the physical property of receiver coils.

in Eq. (16) are roughly in the same order. (b) Since the sensitivity function is in general smoother than the image, the parameter β should be orders of magnitude larger than α to impose a stronger smoothness constraint.

4. Results

4.1. Simulation

To study the effectiveness of the proposed method under noise-free measurements, we have compared the SOS, MAP-MBD, p-norm, Subspace-MBD, and ML-MBD methods using simulated data. Fig. 1 presents the true image and the reconstructed images obtained from the SOS, MAP-MBD, p-norm, Subspace-MBD and ML-MBD methods, together with the difference images between each reconstructed image and the true image. Fig. 2 shows the sum-of-squares of the corresponding sensitivity functions. It is observed in Fig. 1 that the center part of the SOS reconstruction is much darker compared to that of the other methods. This is because the SOS reconstruction is based on the assumption that the sum of square of the sensitivity functions is a constant. However, as shown in Fig. 2, this assumption is clearly violated for the sensitivity functions. Similarly, neither the image nor the sensitivities obtained by the Subspace-MBD method resemble the true ones. In contrast, the sum-of-squares of the estimated sensitivity functions obtained by the MAP-MBD, p-norm and ML-MBD methods is non-uniform and resembles that of the true one. It suggests that in the noise-free case, the proposed method performs similar to the p-norm and ML-MBD methods.

4.2. Phantom experiment

For the phantom data, Fig. 3 presents the reconstructed images using four different methods. We observe that the intensity of reconstruction using the proposed method is more uniform across the whole image, when compared with the SOS reconstruction, which is very dark in the center, the p-norm method, which is non-uniform around the center, the Subspace-MBD method, which is clearly non-uniform along the vertical direction, and the ML-MBD method, which is also non-uniform around the center.

4.3. In vivo human brain imaging experiment

Reconstructions for the *in vivo* human brain data are shown in Fig. 4. The intensity of the reconstruction by the proposed MAP-MBD method is more uniform across the whole image, when compared with those by the SOS, p-norm, Subspace-MBD, and ML-MBD

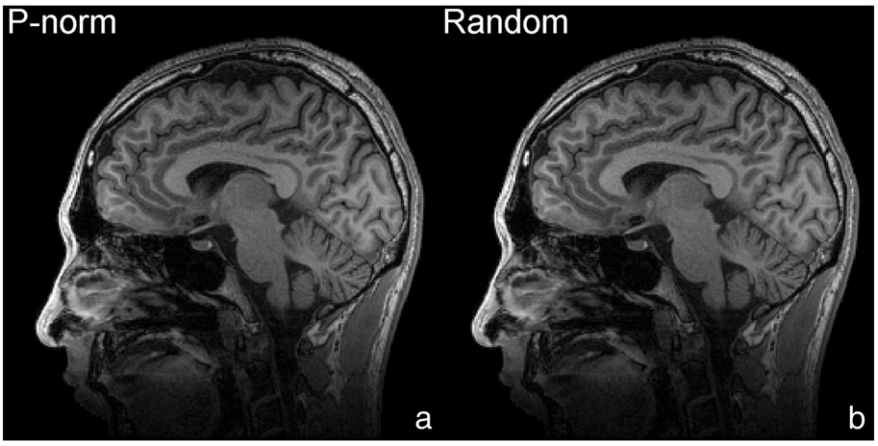

Fig. 6. Comparison of random initialization and p-norm initialization. Both initialization methods lead to similar reconstructions.

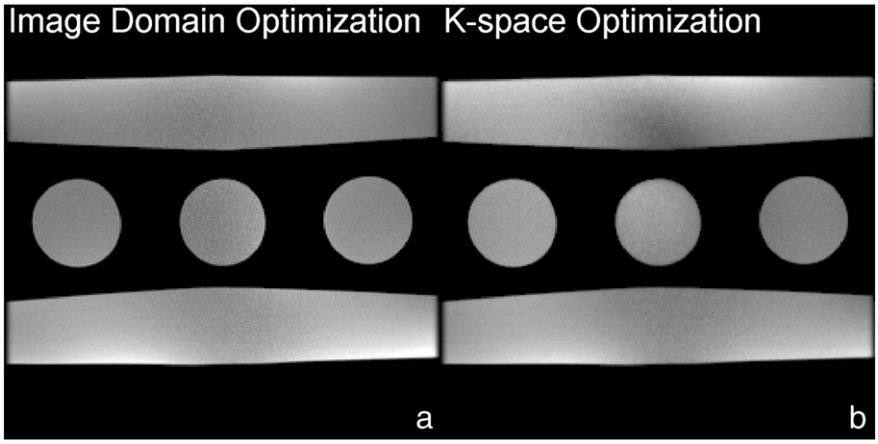

Fig. 7. Comparison of image-domain and *k*-space reconstructions. Image domain method provides more uniform intensity across the image.

methods. In particular, the central upper region of the brain image is sharper than that in the SOS reconstruction. The Subspace-MBD method is unable to provide a uniform reconstruction, possibly due to its lack of robustness to noise. The p-norm and ML-MBD reconstructions are seen to be much noisier compared with the proposed MAP-MBD reconstruction.

4.4. In vivo cardiac imaging experiment

Reconstructions for the *in vivo* cardiac data are shown in Fig. 5. The intensity of the reconstruction by the proposed MAP-MBD method is more uniform across the image, when compared with those by the SOS and Subspace-MBD methods. The p-norm and ML-MBD reconstructions are much noisier than those of the proposed method. The sensitivity reconstructions of one coil near the air–tissue interface for all methods are also shown in Fig. 5. While the true sensitivity is unknown, the MAP-MBD estimation gives a smoother and cleaner estimation of the sensitivity than that of the other methods over the entire FOV. This agrees with the physical property of the receiver coil sensitivity [3,13,19].

5. Discussion

5.1. Relation to previous works

As introduced earlier, the proposed MAP-MBD method is a regularized version of ML-MBD method. When the regularization parameters α and β of MAP-MBD method are set to be zero, the MAP-MBD method becomes ML-MBD. Without the regularization terms, the solution of ML-MBD method may reach some local minimum which might be far away from the true image. The comparisons of MAP-MBD and ML-MBD reconstructions in Figs. 1–5 demonstrate the superior performance of MAP-MBD over ML-MBD.

It is also worth noting that the first iteration of proposed method is similar to the p-norm method. Both methods aim to find the optimal sensitivities among the infinitely many possible solutions. However, the p-norm method terminates without further utilizing the reconstructed image to improve the sensitivities or vice versa. In contrast, the proposed method improves the image and sensitivities through AM iterations. Such AM optimization method can be proved to converge to a local minimum [21], which gives a suboptimal solution to the original nonconvex problem.

5.2. Initialization

The proposed method is robust to different initializations. We have studied random initialization with noise like image and sensitivities as well as initialization with the p-norm combination. Fig. 6 compares the results of random initialization and p-norm initialization. We can see that both initialization methods lead to similar reconstructions.

5.3. Convergence and computation complexity

The proposed method converges fast and only needs 6–8 AM iterations. In the reconstruction of the sagittal brain dataset, the computer running time is around 120 s (for 6 AM iterations). We have also previously investigated the k-space implementation of the

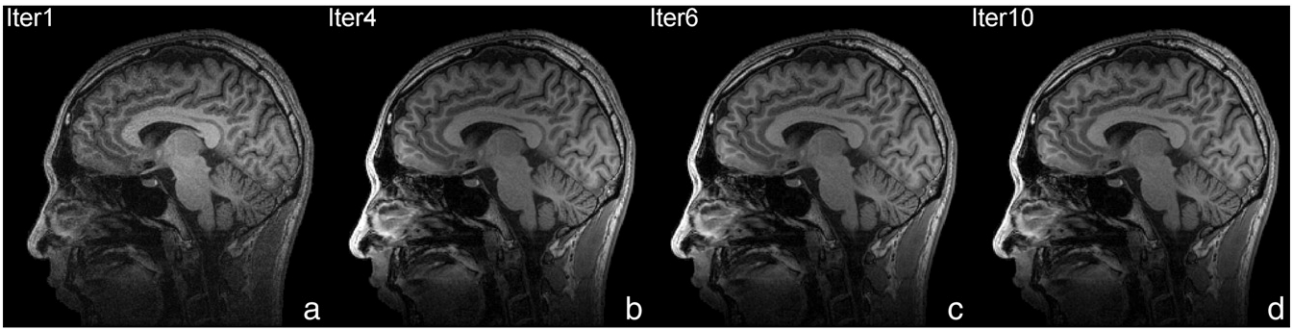

Fig. 8. Reconstructions of the proposed method for the 1st, 4th, 6th, and 10th iterations. After the 1st iteration, the reconstruction is seen to be close to the p-norm result, and after 4 iterations, the uniformity is improved. Further iterations do not improve the uniformity much.

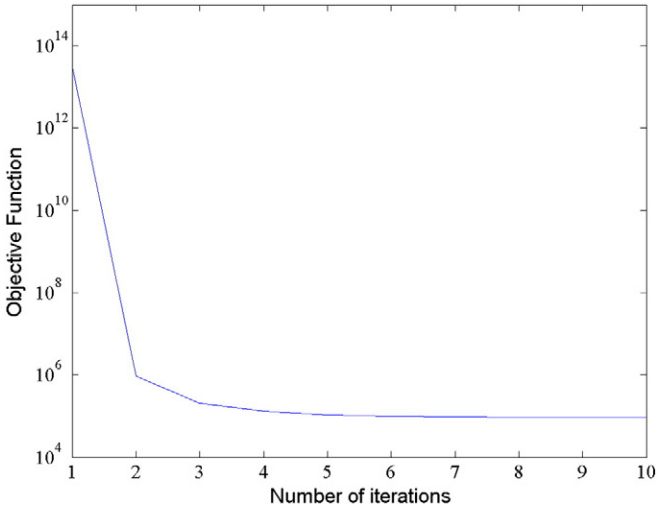

Fig. 9. Convergence curve showing the value of the objective function of the proposed method is decreasing more rapidly at the first few iterations, but remains almost unchanged afterwards.

proposed method, which was partially reported in [22]. The k-space method takes more than 600 s for the same set of sagittal brain data. The reconstruction results of the image domain method and the *k*-space method are also compared in Fig. 7. We can see that, for this phantom dataset, the image-domain method improves the reconstruction uniformity when compared with the *k*-space method. In addition, the objective function decreases rapidly during the beginning iterations. After that the algorithm converges and further iterations do not improve the quality of reconstruction. This is demonstrated in Fig. 8 for the *in vivo* brain data, where the first iteration still gives inhomogeneous and noisy image, while the 4th iteration reconstruction appears uniform, and the 6th iteration and 10th iteration show little difference from the 4th iteration. Fig. 9 shows the objective function $E(\vec{f}, \vec{h}_i)$ versus the number of iterations for the optimization. $E(\vec{f}, \vec{h}_i)$ decreases till convergence after 6 iterations, which matches the observation in Fig. 8.

5.4. Signal-to-noise ratio

In addition to the uniformity of intensity, the SNR of the final reconstruction is also improved over the SOS, p-norm and ML-MBD reconstructions due to the regularization terms for both image and sensitivities in the proposed method. We can observe the improvement of SNR for the proposed method over SOS, p-norm and ML-MBD reconstructions in Figs. 4 and 5 as discussed in the Results section.

5.5. Smaller FOV imaging

In practice, sometimes the field of view (FOV) is slightly smaller than the selected object, causing a small overlap in the acquired image [23,24]. In this case, the estimated coil sensitivities might have sharper features than those of the case with full FOV. In the following, we simulate such a scenario based on the cardiac data in Fig. 5. First, we shift each coil's image up and down by several pixels and then add the shifted images to the original image. Next, we truncate the summation images to a reduced FOV to construct a case in which the FOV is slightly smaller than the selected object and thus aliasing occurs. The reconstructions are shown in Fig. 10, where the overlap occurs at the top and bottom of the image. The conclusion remains the same that the proposed MAP-MBD method can still reconstruct cleaner images than those of the p-norm and ML-MBD methods, and more uniform images than the Subspace-MBD method. The estimated sensitivity map by the MAP-MBD method also gives a smooth estimation over the entire FOV, which agrees with the physical property of receiver coils.

6. Conclusion

In this paper, we develop a regularized MAP-MBD method for image reconstruction using multichannel phased-array MRI data. The proposed method is compared with SOS, Subspace-MBD, p-norm, and ML-MBD methods using phantom and *in vivo* experiments. The results demonstrate that the proposed method reconstructs more uniform images than the SOS does. It is also more robust than the Subspace-MBD approach in the presence of measurement noise. The proposed method provides more uniform images than the SOS and Subspace-MBD methods, and improves SNR of the p-norm and ML-MBD methods.

Acknowledgments

The authors would like to thank Dr. Filip Šroubek for helpful discussions and for making available the MBD MATLAB code at http://zoi.utia.cas.cz/download. This work is supported in part by the National Science Foundation CBET-1265612 and ECS-0547433.

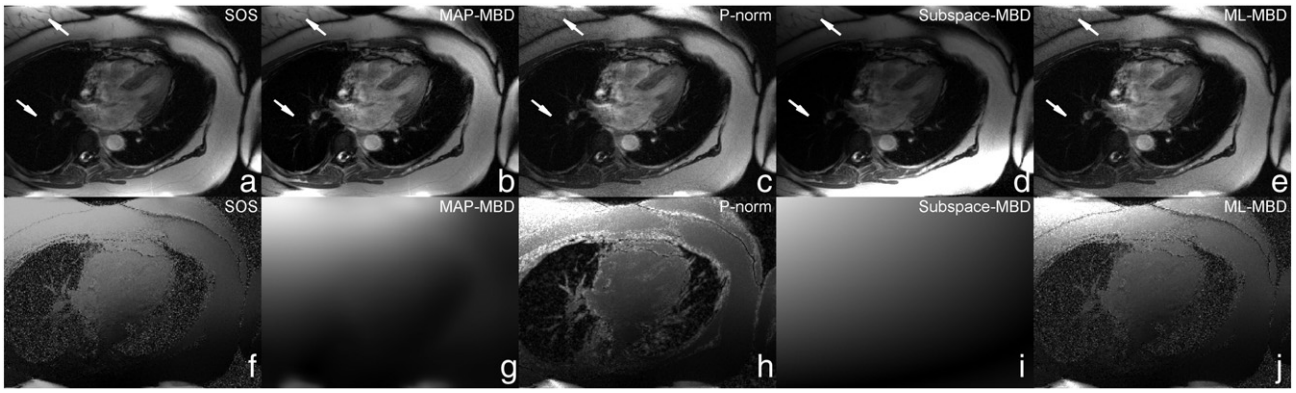

Fig. 10. Simulation results based on modified *in vivo* cardiac data used in Fig. 5. The top row shows the reconstructions and the bottom row shows the sensitivity maps. The FOV is slightly smaller than the selected object, causing a small overlap in the acquired image (at the top and bottom). The proposed MAP-MBD method can still reconstruct less noisy images than the p-norm and ML-MBD methods, and more uniform images than the Subspace-MBD method. The MAP-MBD method also gives a smooth estimation of coil sensitivities in the entire FOV.

References

[1] Roemer PB, Edelstein WA, Hayes CE, Souza SP, Mueller OM. The NMR phased array. Magn Reson Med 1990;16:192–225.
[2] Sodickson DK, Manning WJ. Simultaneous acquisition of spatial harmonics (SMASH): fast imaging with radiofrequency coil arrays. Magn Reson Med 1997; 38:591–603.
[3] Pruessmann KP, Weiger M, Scheidegger MB, Boesiger P. SENSE: sensitivity encoding for fast MRI. Magn Reson Med 1999;42:952–62.
[4] Griswold MA, Jakob PM, Heidemann RM, Nittka M, Jellus V, Wang J, et al. Generalized autocalibrating partially parallel acquisitions (GRAPPA). Magn Reson Med 2002;47:1202–10.
[5] Kellman P, McVeigh ER. Ghost artifact cancellation using phased array processing. Magn Reson Med 2001;46:335–43.
[6] Axel L, Constantini J, Listerud J. Intensity correction in surface-coil MR imaging. AJR Am J Roentgenol 1987;148:418–20.
[7] Murakami JW, Hayes CE, Weinberger ED. Intensity correction of phased-array surface coil images. Magn Reson Med 1996;35:585–90.
[8] Debbins JP, Felmlee JP, Riederer SJ. Phase alignment of multiple surface coil data for reduced bandwidth and reconstruction requirements. Magn Reson Med 1997;38:1003–11.
[9] Bydder M, Larkman DJ, Hajnal JV. Combination of signals from array coils using image-based estimation of coil sensitivity profiles. Magn Reson Med 2002;47: 539–48.
[10] Walsh DO, Gmitro AF, Marcellin MW. Adaptive reconstruction of phased array MR imagery. Magn Reson Med 2000;43:682–90.
[11] Hadjidemetriou S, Studholme C, Mueller S, Weiner M, Schuff N. Restoration of MRI data for intensity non-uniformities using local high order intensity statistics. Med Image Anal 2009;13:36–48.
[12] Çukur T, Lustig M, Nishimura DG. Multiple-profile homogeneous image combination: application to phase-cycled SSFP and multicoil imaging. Magn Reson Med 2008;60:732–8.
[13] Morrison RL, Jacob M, Do MN. Multichannel estimation of coil sensitivities in parallel MRI. IEEE Int Symp Biomed Imaging 2007:117–20.
[14] Hua Y. Fast maximum likelihood for blind identification of multiple FIR channels. IEEE Trans Signal Process 1996;44:661–72.
[15] Gurelli M, Nikias C. EVAM: an eigenvector-based algorithm for multichannel blind deconvolution of input colored signals. IEEE Trans Signal Process 1995;43: 134–49.
[16] Harikumar G, Bresler Y. Perfect blind restoration of images blurred by multiple filters: theory and efficient algorithms. IEEE Trans Image Process 1999;8:202–19.
[17] Šroubek F, Cristóbal G. A unified approach to superresolution and multichannel blind deconvolution. IEEE Trans Image Process 2007;16:2322–32.
[18] Ying L, Liu B, Steckner MK, Wu G, Sheng J, Wu M, et al. A statistical approach to SENSE regularization with arbitrary trajectories. Magn Reson Med 2008;60: 414–21.
[19] Ying L, Sheng J. Joint image reconstruction and sensitivity estimation in SENSE (JSENSE). Magn Reson Med 2007;57:1196–202.
[20] Ulaby FT. Fundamentals of applied electromagnetics. 5th ed. Prentice Hall; 2006.
[21] She H, Chen RR, Liang D, Chang YC, Ying L. Image reconstruction from phased-array MRI data based on multichannel blind deconvolution. IEEE Int Symp Biomed Imaging 2010:760–3.
[22] Chan TF, Wong CK. Convergence of the alternating minimization algorithm for blind deconvolution. Linear Algebra Appl 2000;316:259–85.
[23] Bernstein MA, King KF, Zhou XJ. Handbook of MRI pulse sequences. Elsevier; 2004.
[24] James WG. The SENSE Ghost: field-of-view restrictions for SENSE imaging. J Magn Reson Imaging 2004;20:1046–51.